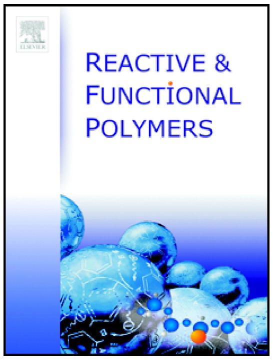

ROMP polymer supported manganese porphyrins: Influence of CC bonds along polymer chains on catalytic behavior in oxidation of low concentration Fe2+

Fanfan Li, Xuan Wang, Huanhuan Zhao, Yanwu Zhang

PII: S1381-5148(19)31269-6

DOI: https://doi.org/10.1016/j.reactfunctpolym.2020.104530

Reference: REACT 104530

To appear in: *Reactive and Functional Polymers*

Received date: 27 November 2019

Revised date: 8 February 2020

Accepted date: 10 February 2020

Please cite this article as: F. Li, X. Wang, H. Zhao, et al., ROMP polymer supported manganese porphyrins: Influence of CC bonds along polymer chains on catalytic behavior in oxidation of low concentration Fe2+, *Reactive and Functional Polymers* (2019), https://doi.org/10.1016/j.reactfunctpolym.2020.104530

ROMP Polymer Supported Manganese Porphyrins: Influence of C=C Bonds along Polymer Chains on Catalytic Behavior in Oxidation of Low Concentration Fe^{2+}

*Fanfan Li, Xuan Wang, Huanhuan Zhao and Yanwu Zhang**

School of Chemical Engineering and Energy, Zhengzhou University, 100# Science Road, Zhengzhou, 450001, P.R. China

*Corresponding author.

**E-mail address: zhangyanwu@zzu.edu.cn*

ABSTRACT

One unsaturated polymer support was prepared through ring opening metathesis polymerization (ROMP) of norbornene-2,3-dip-toluene sulfonate initiated by Grubbs 2nd initiator and manganese porphyrins were immobilized on polymer through transesterification reaction. To investigate the effect of C=C bonds along polymer chains on the catalytic behavior, the obtained polymer supported catalyst (P-PPIXMnCl) was applied in oxidation of low concentration Fe^{2+} to mimic catalytic behavior of Ceruloplasmin. In the presence of P-PPIXMnCl, the conversion of Fe^{2+} reaches to 91.92% and 96.46% at 10 °C and 37.5 °C (body temperature), respectively. Compared to manganese porphyrins, P-PPIXMnCl can dramatically increase oxidation rate of Fe^{2+} and the catalytic kinetic shows that the oxidation reaction changes from second-order to third-order. Upon hydrogenation of ROMP polymer, the oxidation reaction still conforms to the second-order kinetics. Density functional theory (DFT) calculation shows that the C=C bonds along polymer chains play an important role in the coordination with Fe^{2+} in the catalytic microenvironment. The real time morphology of supported catalysts in aqueous environment characterized by Cryo-TEM indicates that hydrogenation can shrink the morphology of polymer-water skeleton. The catalyst could be recycled six times without any significant loss in activity. The liner heterogeneous catalyst is expected to be used as drugs for treating excessive iron accumulation in the human body.

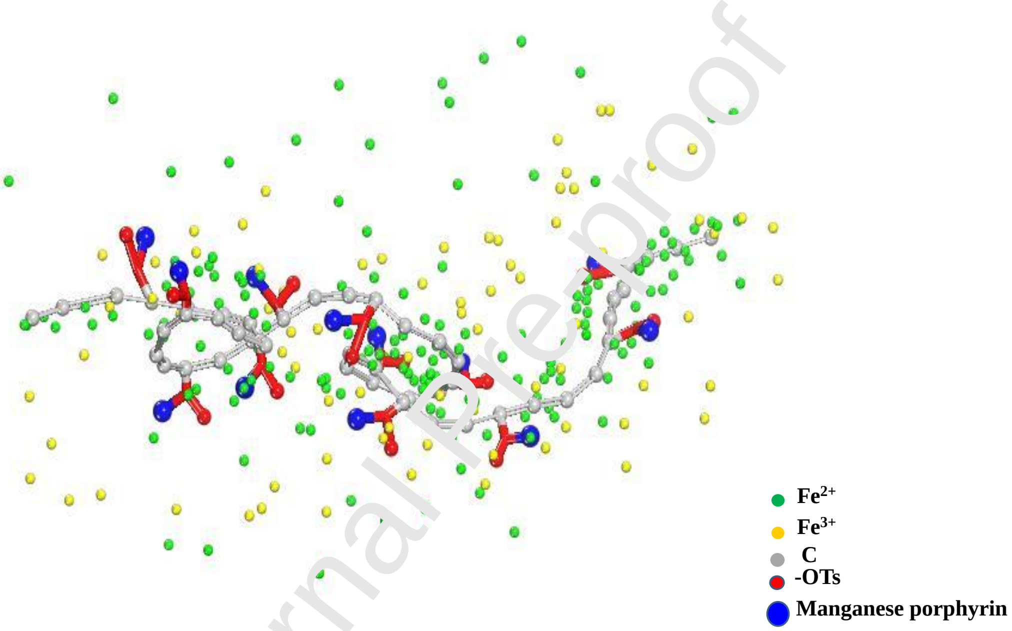

Keywords: Ring-opening metathesis polymerization; Polymer support; Manganese porphyrins; Bionic catalyst; Catalytic oxidation; Cryo-TEM

1. Introduction

In the organism, natural oxidase surrounded by polypeptides can fully play the catalytic effect in the local hydrophobic microenvironment that formed by polypeptide chains. Similarly, macromolecular chains provide the bionic hydrophobic microenvironment in catalytic process when catalysts are supported on macromolecules. This kind of biomimetic microenvironment can not only protect the catalyst from the destruction and deactivation caused by autoxidation and aggregation, but also improve activity and selectivity of catalysts [1-4].

According to the principle of enzyme catalysis in life, the bionic chemical catalysts are designed to mimic some active groups or parts in the biocatalysts [5-7]. Iron is a necessary metal element for human body, and it plays an important role in oxygen transport, cell biological oxidation, DNA replication and electron transfer. The blood circulation process is dependent on oxidization of Fe^{2+} catalyzed by serum Ceruloplasmin (Cp) and transferrin Helper Protein (Hephaestin) [8, 9]. In the oxidation process of Fe^{2+}, Fe^{2+} ions firstly replace Cu^{2+} ions in Cp and then Fe^{2+} ions are oxidized to Fe^{3+} ions [10-13]. When Cp is deficient or incapacitated, it can cause iron deposition in local tissues [14]. Therefore, a bionic catalyst simulating the function of Cp in the oxidation of Fe^{2+} is required to treat disease arising from deficiency or a function of Cp. In order to explore the influence of the microenvironment formed by polymers on the biomimetic catalytic mechanism, oxidation of Fe^{2+} in the presence of polymer-supported catalyst mimicking Cp was studied.

Over the last decades, metalloporphyrins have been successfully used as models for the cytochrome P-450 enzymes. Porphyrins and metalloporphyrins with a large conjugated ring structure are widely applied in catalysis, special materials and targeted drugs [15, 16]. However, the catalytic efficiency of porphyrins will be reduced due to agglomeration in normal conditions [17-19]. Many studies have shown that anchoring metalloporphyrins on suitable carrier materials can improve catalyst activity, stability and product selectivity owing to the support environment. The common inorganic carriers include activated carbon, montmorillonite, silica, zeolite and molecular sieve [20-25]. Further, organic carriers such as polystyrene and resins are also used to immobilize metalloporphyrins [26, 27]. Among all kinds of solid scaffolds, polymer scaffolds have attracted much attention due to their inherent characteristics. Compared to rigid inorganic carriers, polymer with abundant conformations can build a flexible catalytic microenvironment formed by C=C bonds along polymer chains and therefore catalytic activity and stability of metalloporphyrins can be improved obviously [28-31]. Ring-opening metathesis polymerization (ROMP) has high functional group tolerance initiated by Grubbs catalysts and is widely applied in synthesis of well-defined polymers [32-36]. The living features of ROMP are helpful to design and synthesize advanced structures such as metallocarbene-containing polymers, functional nanoparticles and topologic polymers [37-42].

For mimicking the natural enzyme, designing the skeleton of the model to select the access of the substrate to metal center is a crucial object [43]. In our previous work, one bifunctional chelating supramolecular polymer was prepared to down-regulate cellular iron uptake through chelating and reduction of Fe^{3+} [44]. Moreover, the catalytic oxidation of Fe^{2+} to Fe^{3+} by manganese complexes was previously reported [45-47]. Herein, we immobilized manganese porphyrins onto linear polymer and catalyzed oxidation of low concentration Fe^{2+}. To simulate polypeptide of Cp, polymer support was synthesized by ROMP of 5-norbornene-2,3-dip-toluene sulfonate (NDT), π electrons of double bonds along the polymer chains provided coordination sites of Fe^{2+} ions. Manganese porphyrins as active sites were immobilized on poly (5-norbornene-2,3-dip-toluene sulfonate) (PolyNDT) through transesterification reaction (Complete experimental process is shown in Scheme 1). The catalytic behavior of supported manganese porphyrins (P-PPIXMnCl) at low temperature in oxidation of low concentration Fe^{2+} was studied. The microscopic images obtained under vitrified, frozen hydrated condition confirm the state of the catalyst in the water environment analyzed by Cryo-TEM imaging technique [48-50]. DFT method was used to calculate the interaction energy between Fe^{2+} and polymer.

2. Experimental

2.1. Materials

The Grubbs 2nd catalyst (Sigma-Aldrich) and ethyl vinyl ether (98%, TCI), cis-5-norbornene-endo-2,3-diacid anhydride (99%, J&K), dicyclopentadiene (99%, J&K), maleic anhydride (95%, Sigma-Aldrich), methyl tert-butyl ether (99%, J&K), lithium aluminium hydride (97%, Sigma-Aldrich), 4-

dimethylaminopyridine (DMAP, 99%, J&K), pyridine (99%, Sigma-Aldrich) was used after distillation. Tetrahydrofuran (THF), anhydrous ether and dichloromethane (CH_2Cl_2) were used after refluxed onto sodium or calcium hydride, 4-toluene sulfonyl chloride (99%, J&K), hemin (95%, J&K), benzene (99.5%, J&K), tributyl phosphate (TBP, 99%, Sigma-Aldrich). $MnCl_2 \cdot 4H_2O$ (98%, TCI), N,N-Dimethylformamide (DMF, 99.9%, Sigma-Aldrich), $FeSO_4 \cdot 7H_2O$ (99.9%, Sigma-Aldrich), H_2O_2 (31%, Sigma-Aldrich).

2.2. Characterization

^{1}H NMR spectra was recorded on Bruker AV 400 spectrometer with Si $(CH_3)_4$ as an internal standard. Gel permeation chromatography (GPC) measurement was carried out by an Agilent 1100 series equipped with an RI-G1362A RI detector and a PL gel Mixed-C column using DMF as the mobile phase at a flow rate of 1.0 mL·min^{-1} at 25 °C. UV-Visible (UV-Vis) absorption measurement was carried out on Shimadzu UV-2450 spectrometer. Fourier Transform-Infrared Spectroscopy (FT-IR) was recorded on an FT-IR Nicole spectrometer over the range of 4000-500 cm^{-1}. Inductively Coupled plasma mass spectrometry (ICP-MS) measurement was carried out with Optimass 9500 NWR-213. Elemental Analyzer (EA) was carried out on vario EL III. The transmission electron microscopy (TEM) was observed by FEI TalosF200S. Cryo-Transmission Electron microscopy (Cryo-TEM) was observed by Talos F200C 200KV.

2.3. Experiment

2.3.1. Preparation of PolyNDT

In a vacuum glove box, Grubbs 2nd catalyst (0.009 g, 0.01 mmol) was dissolved in dichloromethane (1 mL), and then the solution was added in a single flask and stirred for 15 minutes at 25 °C. After that, the monomer NDT (0.460 g, 3 mmol) dissolved in dichloromethane (15 mL) was added in flask, the mixture was stirred for 6 h at 25 °C. Subsequently, the terminator vinyl ether (600 equiv) was added and the stirring was continued for 0.5 h. After the reaction, the mixture was added into the cold ether (100 mL) and the light yellow solid was precipitated. Then the precipitate was dissolved in THF, and the polymer solid was got again with ether as precipitator. Then the solid product was dried in vacuum at 25 °C to obtain the PolyNDT (0.228 g). Yield: 91%.

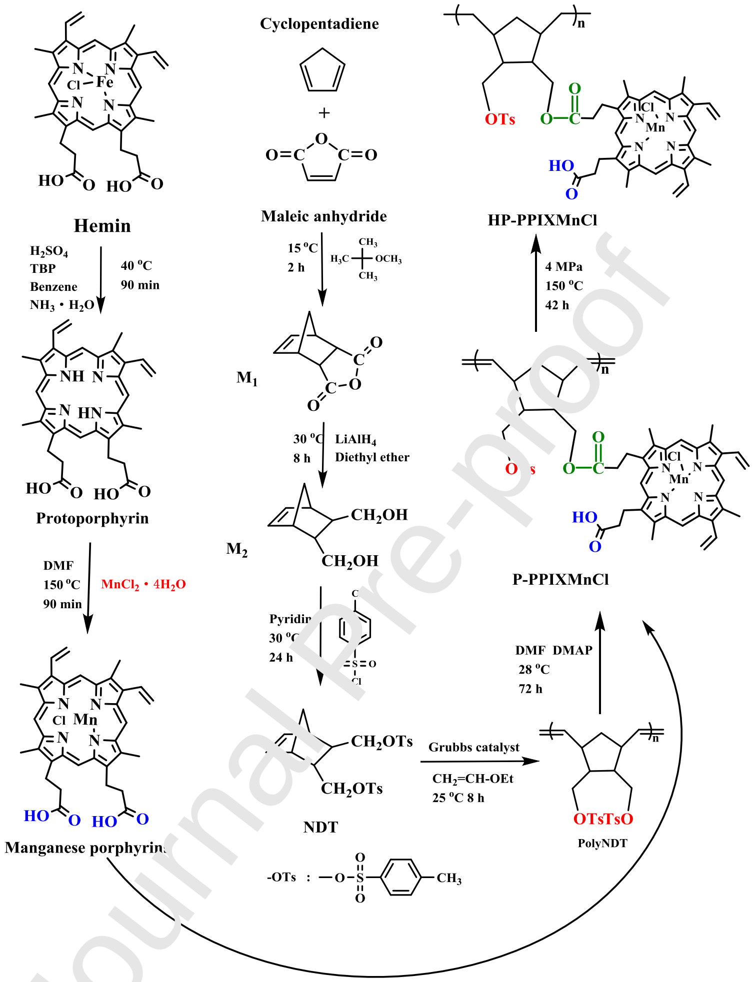

Scheme 1. Manganese porphyrins immobilized on PolyNDT and HPolyNDT.

2.3.2. Synthesis of P-PPIXMnCl

PolyNDT (0.560 g, 1.2 mmol) was dissolved in DMF (100 mL). Then the mixture was added into three-necked flask. Manganese porphyrins (0.225 g, 0.4 mmol) and DMAP (0.015 g, 0.12 mmol) were added, the compound was stirred for 3 days at 28 °C. After the reaction, the crude product was washed by CH_2Cl_2 (100 mL × 3) and water (100 mL × 3) respectively. After centrifugation and vacuum drying at 50 °C, then the dark product was obtained (0.644 g). Yield: 82%.

2.3.3. Hydrogenation of PolyNDT

PolyNDT was dried for 24 h at 80 °C to remove trace moisture before the experiment. Then, PolyNDT dissolved in DMF was placed in a high pressure hydrogenation reactor. N_2 was used to purge the reactor for 0.5 h firstly. Afterwards, the reaction solution was gradually heated to 150 °C under the hydrogen pressure 1 MPa. H_2 was continuously filled until the pressure in the reactor reached 4 MPa. After 42 h of reaction, the liquid was cooled to room temperature before the reaction device was de-compressed. And then the mixture was taken out and removed solvent by rotary evaporation, the Hydrogenated PolyNDT (HPolyNDT) was got.

The method that loaded manganese porphyrins on the HPolyNDT was consistent with the above mentioned process 2.2, and the product HP-PPIXMnCl was obtained.

2.3.4. Catalytic oxidation of Fe^{2+} to Fe^{3+}

$FeSO_4 \cdot 7H_2O$ was dissolved in 10 mL distilled water. 5 mL of the solution was fixed volume in 1 L volumetric flask. And then 15 clean reaction bottles (20 mL) were marked as 10-0, 10-1, 10-2, 20-1, 20-1, 20-2, 30-0, 30-1, 30-2, 40-0, 40-1, 40-2, 50-0, 50-1 and 50-2. 10 mg (n (Mn^{3+}) = 15.38 μmol) manganese porphyrins were added in the reaction bottles which labeled 10-1, 20-1, 30-1, 40-1 and 50-1. And 10 mg (n (Mn^{3+}): 10.98 μmol) P-PPIXMnCl was added in the reaction bottles which labeled 10-2, 20-2, 30-2, 40-2 and 50-2. 15 mL of Fe^{2+} solution (3.53 μmol/L) was added into all reaction bottles, and each bottle was injected with 50 μL 30% H_2O_2 (32.65 mmol/L). Then the mixture was homogenized by magnetic stirrer at 10 °C. Reaction time of the solution in bottles which labeled 10-0, 10-1 and 10-2 was 10 minutes; in 20-0, 20-1 and 20-2 was 20 minutes; 30-0, 30-1 and 30-2 was 30 minutes; 40-0, 40-1and 40-2 was 40 minutes, and 50-0, 50-1 and 50-2 was 50 minutes. At the end of the reaction, the compounds in flasks which labeled 10-1, 10-2, 20-1, 20-2, 30-1, 30-2, 40-1, 40-2, 50-1and 50-2 were filtered. Reaction processes are shown in Scheme 2.

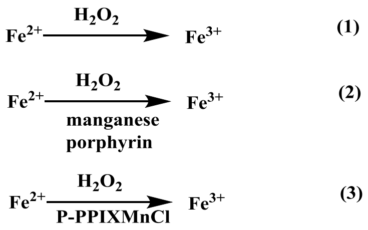

Scheme 2. Catalytic oxidation of Fe^{2+}.

2.4 Computational methods

As a complement to experimental results, DFT calculation is a powerful method to understand the geometry structure and interaction between catalyst and reactant. The DFT studies on catalytic oxidation of manganese porphyrin have been reported in previous literatures [51].

In this work, interaction energy between Fe^{2+} and P-PPIXMnCl (a)/HP-PPIXMnCl (b) were calculated by Accelrys Material Studio Dmol3 module. Catalyst molecules P-PPIXMnCl (a)/HP-PPIXMnCl (b) and reactant molecule Fe^{2+} were optimized by the GGA and PBE funcational form, DNP (double numeral plus polarization) basis set was used to describe the valence orbitals of the atoms [52]. The convergence criterion of self-consistent field calculation, tolerances of energy, maximum force, and maximum displacement for the geometry optimization were 1×10^{-6} Hartree, 1×10^{-5} au, 0.002 au and 0.005 au, respectively. The interaction energy between Fe^{2+} and polymer was described as:

$$E_{inter} = E_{Fe^{2+}\text{-}polymer} - E_{polymer} - E_{Fe^{2+}}$$

3. Results and discussion

3.1. Materials Characterization

GPC was used to characterize ROMP polymer. Corresponding curves of monomer NDT and polymer PolyNDT are shown in Fig. 1. The shift to left of the characteristic peak in Fig. 1 indicates that the polymerization of NDT is achieved and the calculated PDI value of ROMP polymer is 1.56. The left small shoulder peak is ascribed to the coupling termination of living chains [53]. The polymerization is also proved by ^{1}H NMR spectra in Fig. 2. After ROMP, the position of C=C peaks shifts from 5.93 (a) to 5.32 (a´). The monomer conversion is 54.54% according to the ratio between two characteristic peak areas. The values of M_n, M_w, M_p and PDI of PolyNDT are shown in Table 1.

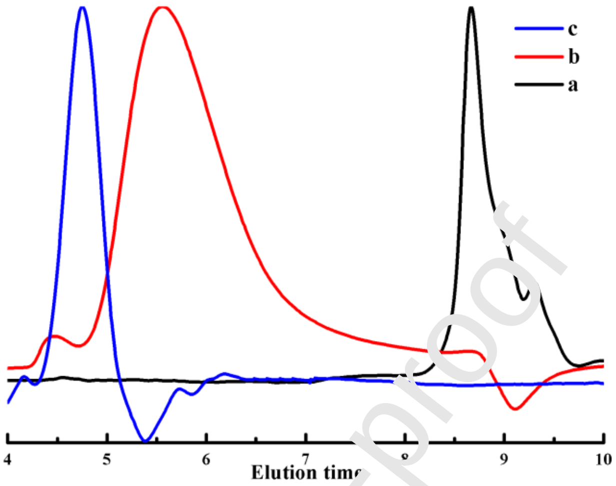

Fig. 1. GPC Curves of NDT (a), PolyNDT (b) and P-PPIXMnCl (c).

Table 1

The values of M_n, M_w, M_p and PDI for PolyNDT and P-PPIXMnCl.

	M_n	M_w	M_p	PDI
PolyNDT	2.6743e5	4.1879e5	4.2163e5	1.56
P-PPIXMnCl	4.2009e6	4.3670e6	4.0194e6	1.04

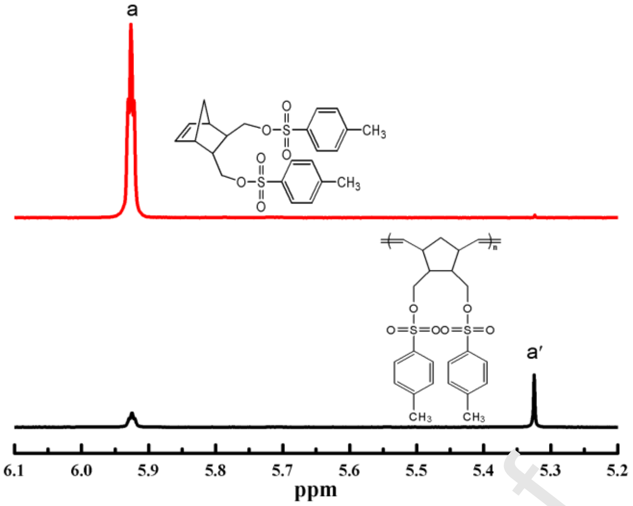

Fig. 2. ^{1}H NMR spectra of comparison between vinyl peaks of NDT and PolyNDT in $CDCl_3$.

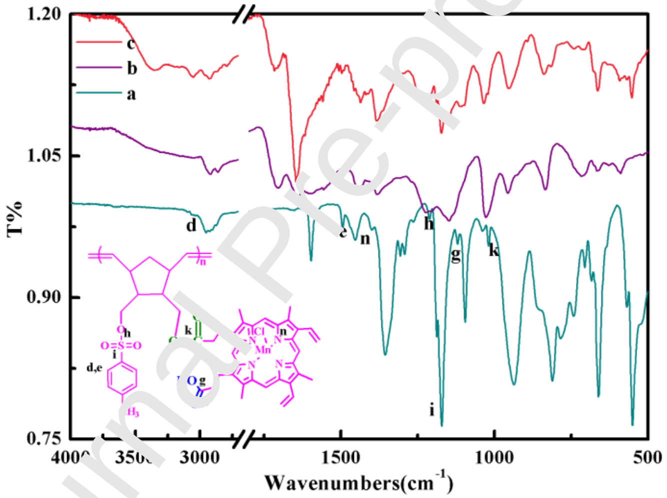

Fig. 3. FT-IR spectra of PolyNDT (a), manganese porphyrin (b) and P-PPIXMnCl (c).

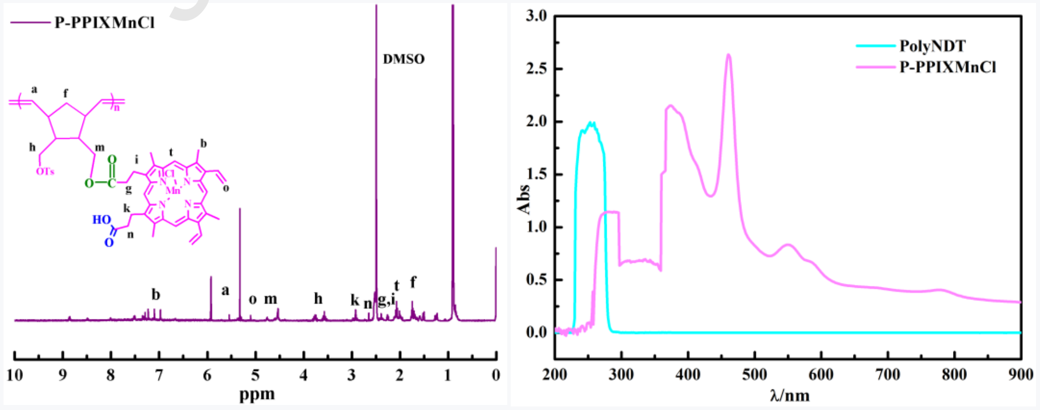

(a)

(b)

Fig. 4. ^{1}H NMR spectrum (a) and UV-Vis spectra (b) of P-PPIXMnCl.

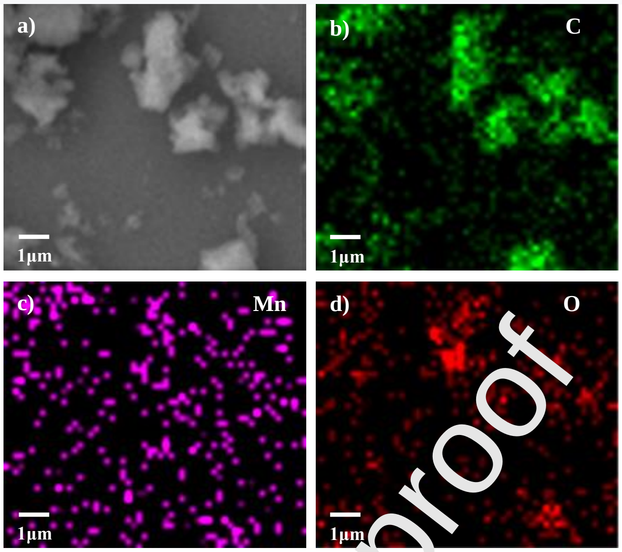

Fig. 5. TEM and EDS mappings of C element (b), Mn element (c) and O element (d) for P-PPIXMnCl.

When manganese porphyrins are immobilized onto PolyNDT, the GPC peak continues to shift to left because of large size of manganese porphyrins in Fig. 1. The values of M_n, M_w, M_p and PDI of P-PPIXMnCl are shown in Table 1. In FT-IR spectra (Fig. 3), 3059 cm^{-1} and 1494 cm^{-1} are attribute to the =C-H and C=C absorption vibration peaks in benzene ring, S-O and S=O stretching vibration peaks appear at 1210 cm^{-1} and 1171 cm^{-1}, respectively. 1121 cm^{-1} belong to C-O stretching vibration peaks, and with characteristic peaks at 1654, 1453 and 1398 cm^{-1} belong to the telescopic vibration absorption peak of C=C and C=N on porphyrin ring. The C-O-C stretching vibration peak at 1019 cm^{-1} is observed and which means manganese porphyrins are successfully immobilized through transesterification reaction. The synthesized P-PPIXMnCl was characterized by ^{1}H NMR. As shown in Fig. 4(a), the ^{1}H NMR spectrum of P-PPIXMnCl displays an absorption peak at 5.07-5.14 ppm, which is the $-CH=CH_2$ (o). Peaks at 1.916-2.177 ppm can be attributed to the chemical displacement of porphyrin ring (t), and the peaks at

6.938-7.372 ppm belong to the absorption peak of at position 2, 7, 12 and 18 in porphyrin ring (b). The chemical displacement of -CH_2- absorption peak (m) that contacts with the ester bond moves to 4.44-4.86 ppm at higher field. The absorption peak at 3.47-3.85 ppm corresponds to the chemical displacement of -CH_2- (h), the characteristic peaks at 2.21-2.31 ppm are ascribed to the -CH_2-CH_2- (g, i) at the position of transesterification, the chemical shifts of -CH_2- (k) and -CH_2- (n) in porphyrin ring appear at 2.82-3.01 ppm and 2.62-2.68 ppm. In addition, the absorption peak at 1.62-2.17 ppm is the -CH_2- signal peak (f) on the main chain, and peak at 5.28-5.39 ppm is attributed to the -CH=CH- (a) on the main chain. So the above analysis indicates successful synthesis of the P-PPIXMnCl. UV-Vis detection was used to characterize PolyNDT and P-PPIXMnCl, and corresponding patterns are shown in Fig. 4(b). It can be seen that P-PPIXMnCl shows a typical characteristic absorption peak (461 nm) at ultraviolet region. This peak exhibits a blue shift compared with the Soret band (481nm) of manganese porphyrin (Fig. S9 line c) and it also has two absorption peaks (551 nm, 777 nm) of Q band for manganese porphyrin at 500-800 nm in the visible region. The absorption band at 283 nm can be ascribed to PolyNDT. Results above provide a further proof that manganese porphyrins had been successfully immobilized on the PolyNDT. Based on the calculation of elemental analysis, the transesterification ratio is 46.90%. In order to indicate the distribution of manganese porphyrins in polymer support, EDS mappings of P-PPIXMnCl are shown in Fig. 5. The consistent distributions of C, Mn and O elements show that manganese porphyrins are successfully loaded on polymer chains.

The synthesis of HPolyNDT and PolyNDT were characterized by ^{1}H NMR. As shown in Fig. 6, the characteristic peaks at 5.2-6.0 ppm are ascribed to C=C in PolyNDT. After hydrogenation, the chemical shift of the C=C in PolyNDT disappears, and the characteristic peaks at 1.69-2.01 ppm appeared which belong to C-C in HPolyNDT backbone. This phenomenon indicates that PolyNDT hydrogenation was completed. The ^{1}H NMR of HP-PPIXMnCl is shown in Fig. 7(a), the absorption peaks at 3.36-3.59 ppm and 4.17-4.53 ppm correspond to the chemical displacement of -CH_2- (h) and -CH_2 (m).

The appearance of new characteristic peaks (-CH_2- (m)) indicates that the esterification reaction has been carried out successfully. The chemical shift of -CH_2- on the main chain appears at 1.79-1.91 ppm. In addition, the absorption peaks at 1.93-2.06 ppm are the chemical displacement of porphyrin ring (t). Results of ^{1}H NMR analysis indicate the successful synthesis of the HP-PPIXMnCl. Fig. 7(b) shows the UV-Vis spectra of HPolyNDT and HP-PPIXMnCl. The Soret band (459 nm) of HP-PPIXMnCl has a blue shift compared with the Soret band (481nm) of manganese porphyrin (Figure S9 line c). In addition, there are two absorption peaks attributed to Q band of manganese porphyrin at 549 nm and 777 nm in the visible region. The absorption band at 279 nm could be assigned to the HPolyNDT. These provide a further proof that manganese porphyrin had been successfully immobilized on the HPolyNDT.

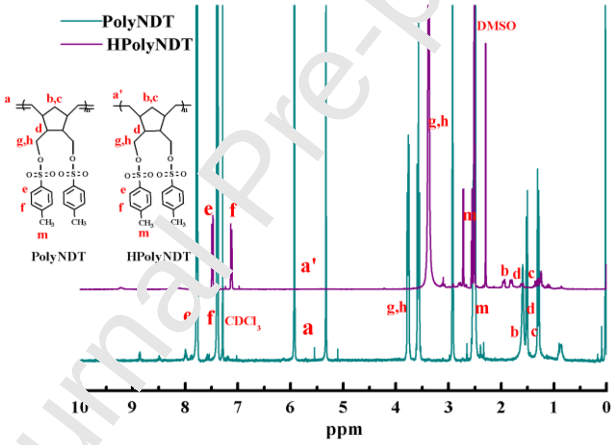

Fig. 6. ^{1}H NMR spectra of HPolyNDT and PolyNDT.

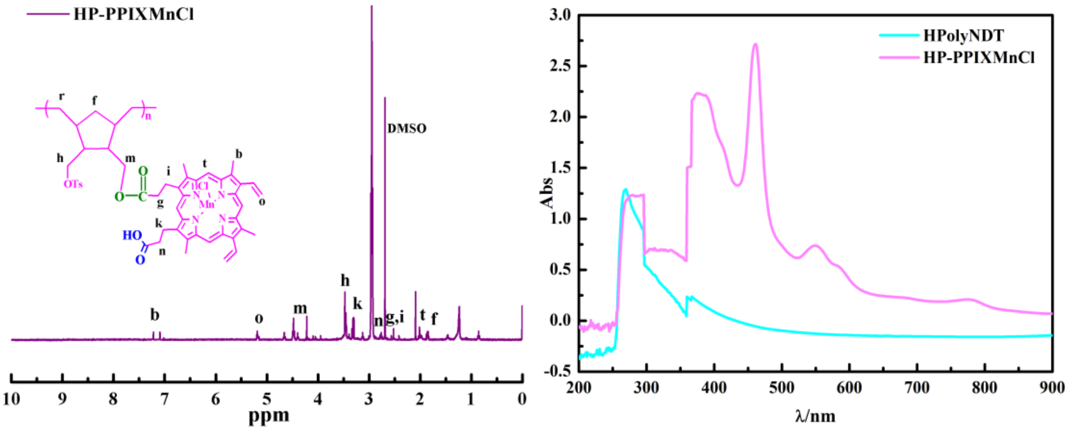

(a) (b)

Fig. 7. ^{1}H NMR spectrum (a) and UV-Vis spectra (b) of HP-PPIXMnCl.

Since the reaction medium of the catalyst is water, the morphological structures of catalyst before and after hydrogenation (P-PPIXMnCl and HP-PPIXMnCl) in water system were analyzed by using Cryo-TEM imaging technique. The microscopic images obtained under vitrified, frozen hydrated condition confirm the state of the catalyst in the water environment, as depicted in Fig. 8. Cryo-TEM analyses allow direct, visual investigation of state of the catalyst in the water environment. In this study, the catalyst structure is retained by freezing and subsequent preservation involved during sample preparation, displaying a dispersion of catalyst (Black structure) in continuous aqueous medium (Gray background).

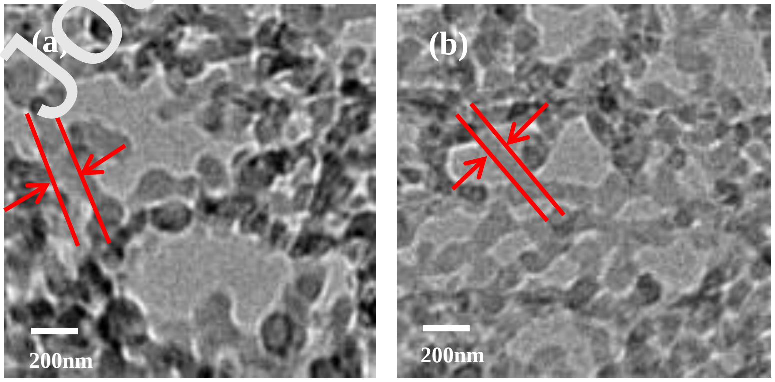

Fig. 8. Cryo-TEM micrographs of P-PPIXMnCl (a) and HP-PPIXMnCl (b).

Fig. 8 shows the Cryo-TEM images of P-PPIXMnCl and HP-PPIXMnCl. It can be seen from Fig. 8 that the skeleton of the hydrogenated catalyst HP-PPIXMnCl is looser than P-PPIXMnCl. This may because that manganese ion interacts with C=C of the skeleton in the catalyst so that making it contract. After hydrogenation, there is a weak interaction between C=C and manganese ion in the catalyst, resulting in a loose skeleton of the catalyst, which indicates that the catalyst provides a flexible microenvironment for the active center. In addition, from Cryo-TEM images, it can be seen that there is a large amount of hydrophilic C=C in the catalyst before hydrogenation, which leads to a thicker skeleton in the water medium. After hydrogenation, there is a lot of C-C with low hydrophilicity in the hydrogenated catalyst, which finally makes the skeleton of HP-PPIXMnCl slightly thinner than that of P-PPIXMnCl.

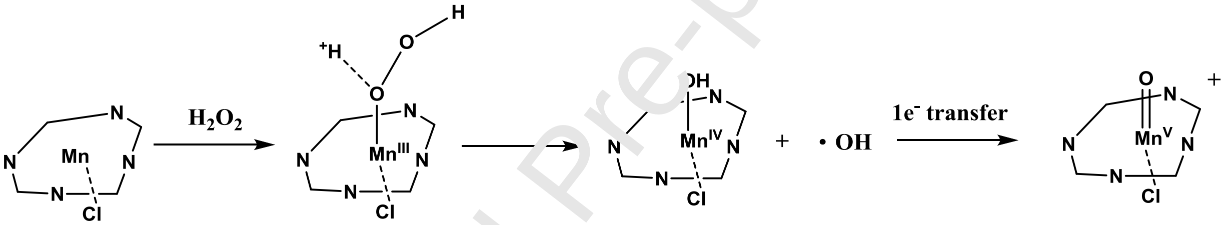

Compound I

Compound II

Compound III

Scheme 3. The likely mode of interaction of manganese porphyrin and H$_2$O$_2$.

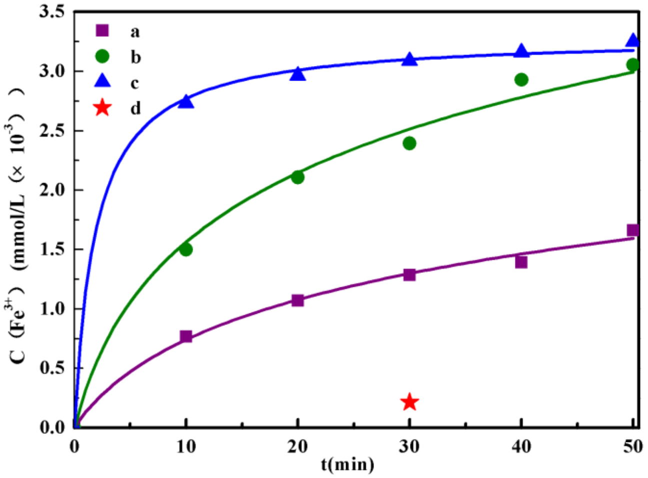

Fig. 9. The curves of C (Fe^{3+})-reaction time t (min) at 10 °C using different catalysts (a, Catalyst - free; b, 10 mg manganese porphyrins (n (Mn^{3+}) = 15.38 μmol); c, 10 mg P-PPIXMnCl (n (Mn^{3+}) = 10.98 μmol).); d, Blank experiment: the degree of oxidation of Fe^{2+} by air.

3.2. Catalytic behavior

As shown in Scheme 3, when H_2O_2 was used as oxidant and metalloporphyrin as catalyst, the intermediate of metalloporphyrin-hydrogen peroxide adduct (Compound I) is produced firstly. And then the hemolysis of O-O bond for Compound I in aqueous solution or aprotic solvent resulted in the formation of Compound II which is a porphyrin oxide intermediate with a hydroxyl radical and single electron. Finally, Compound III is obtained by transferring an electron from the hydroxyl radical [54-58]. To study the catalytic behavior of the supported manganese porphyrins, P-PPIXMnCl is used to catalyze oxidation of low concentration Fe^{2+} and H_2O_2 as oxidizer. The conversion-reaction time curves are plotted in Fig. 9. Both manganese porphyrins and P-PPIXMnCl have good catalytic activity. The conversion of Fe^{2+} in the presence of P-PPIXMnCl rapidly increases to 77.27% in 10 min and is much higher than that of manganese porphyrins. The maximum value of conversion is over 91.92% at 50 min. The remarkable catalytic performance of P-PPIXMnCl is ascribed to the flexible micro-environment for manganese porphyrins built by ROMP polymer. When manganese porphyrins are used, relatively few active sites take part in the reaction because manganese porphyrins are easy to agglomerate. The polymer supporter disperses manganese porphyrins and therefore more sites can take effect. Besides, we did a blank experiment to study the degree of oxidation of Fe^{2+} by air rather than the H_2O_2. Blank experiment indicates that air can oxidize Fe^{2+} slightly in the presence of P-PPIXMnCl, as it shown in Fig. 9 point d.

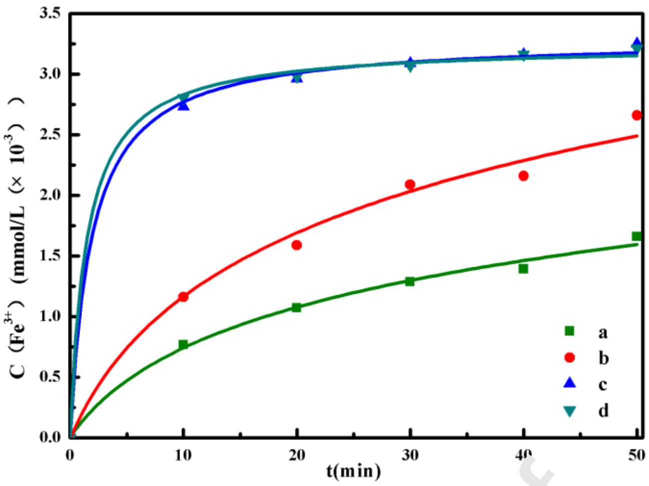

Fig. 10. The curves of C (Fe^{3+})-reaction time t (min) at different amount of catalyst (a, 0 mg P-PPIXMnCl; b, 5 mg P-PPIXMnCl (n (Mn^{3+}) = 5.49 μmol); c, 10 mg P-PPIXMnCl (n (Mn^{3+}) = 10.98 μmol); d, 15 mg P-PPIXMnCl (n (Mn^{3+}) = 16.47 μmol)) at 10 °C.

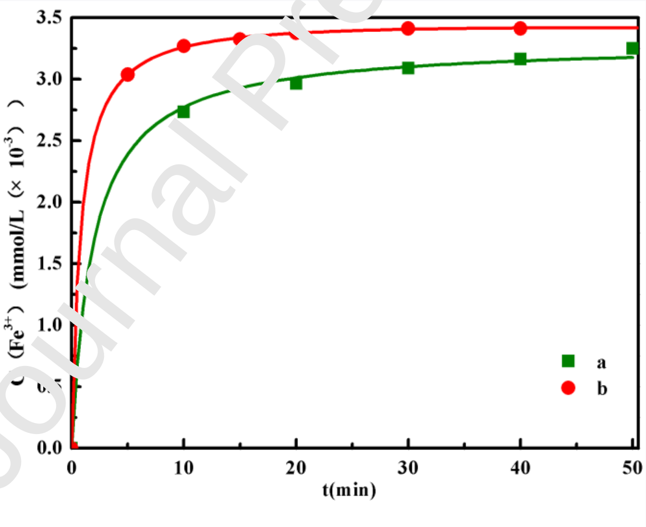

Fig. 11. The curves of C (Fe^{3+})-reaction time t (min) at different temperature (a, 10 °C and b, 37.5 °C) under the catalytic oxidation of 10 mg P-PPIXMnCl (n (Mn^{3+}) = 10.98 μmol).

The catalyst is a key factor in the reaction and directly affects the efficiency of the reaction. As shown in Fig. 10, the conversion of Fe^{2+} increases with the rise of catalyst dosage from 0 mg to 10 mg. However, the conversion of Fe^{2+} did not change much when the catalyst dosage increases from 10 mg to

15 mg. This shows that with the increase of catalytic dosage, the reaction is controlled by diffusion when the amount is small, and the mass transfer efficiency cannot be synchronized when the amount reaches a certain level, the reaction is controlled by activation energy, so the reaction conversion rate no longer changes dramatically with the increase of the catalytic dose. In order to simulate the human body environment, the catalytic oxidation reaction at the human body temperature (37.5 °C) is conducted and the reaction curve is plotted in Fig. 11. The conversion rate of Fe^{2+} at 37.5 °C is faster than that at 10 °C and 96.46% of conversion can be obtained. Therefore, P-PPIXMnCl can work more efficiently at the human body temperature.

To explore the catalytic mechanism of P-PIXMnCl, the apparent kinetics of three reactions processes were studied. The regression lines derived from kinetic data are plotted in Fig. 12 and the corresponding kinetic equations are listed in Table 2. As shown in Fig. 12 and Table 2, the apparent rate constants of different catalysts at the same temperature follow the order: $k_{3(\text{P-PIXMnCl})} > k_{2(\text{Manganese porphyrins})} > k_{1(\text{free catalyst})}$. When the oxidation of Fe^{2+} is catalyzed by manganese porphyrins, the order of reaction is still 2. But the order of reaction increases from 2 to 3 when P-PPIXMnCl is used as catalyst. This indicates that polymer support changes the order of reaction. The parameters of the kinetic curves are shown in Table (A), Table (B) and Table (C) in Fig. 12, respectively. To explain the effect of ROMP polymer on the reaction mechanism, the apparent energy of activation (E_a) and diffusion factor (A) were calculated. The corresponding values are listed in Table 3. Because the catalytic active sites reduce the apparent activation energy, the value of E_a of reaction 2 and 3 is lower than that of reaction 1. In the comparison of reaction 2 and reaction 3, E_a of reaction 2 is less than that of reaction 3 since the number of the active sites in P-PPIXMnCl was lower than manganese porphyrins with the same catalytic dosage; the diffusion factor A is enhanced three orders of magnitude in the presence of P-PPIXMnCl. This is because the dispersion of manganese porphyrins in the flexible polymer conformation leads to a sharp decrease in the diffusion resistance.

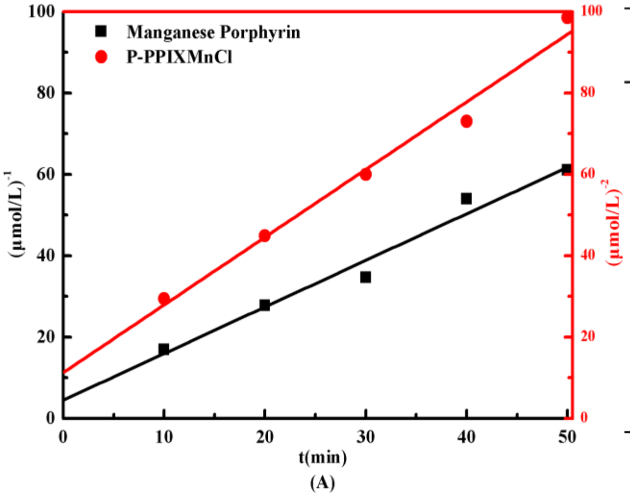

(A)

Equation	y = a + b*x		
Adj. R-Square	0.96713	0.97917	
		Value	Standard Error
Manganese Porphyrin	Intercept	4.5159	3.48449
	Slope	1.14455	0.10506
P-PPIXMnCl	Intercept	11.30415	4.01038
	Slope	1.66264	0.12092

Table (A)

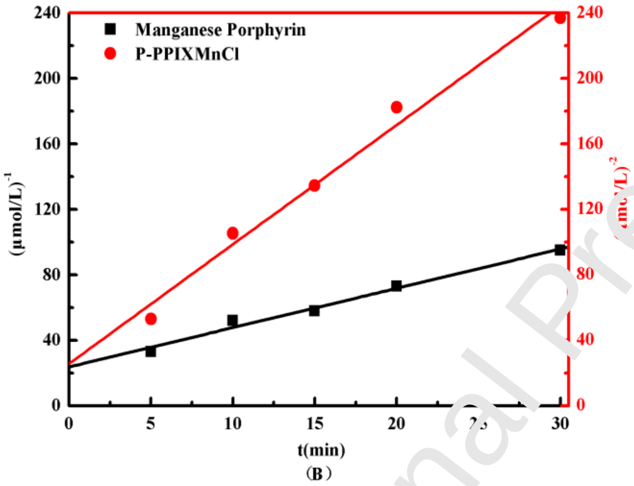

(B)

Equation	y = a + b*x		
Adj. R-Square	0.98105	0.97985	
		Value	Standard Error
Manganese Porphyrin	Intercept	23.75676	3.02588
	Slope	2.4027	0.16657
P-PPIXMnCl	Intercept	25.78686	9.52335
	Slope	7.29321	0.52424

Table (B)

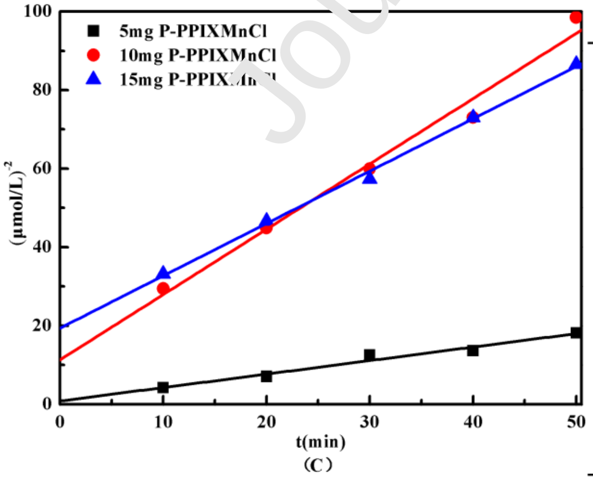

(C)

Equation	y = a + b*x		
Adj. R-Square	0.96452	0.97917	0.99601
		Value	Standard Error
P-PPIXMnCl (5mg)	Intercept	0.80959	1.08742
	Slope	0.34349	0.03279
P-PPIXMnCl (10mg)	Intercept	11.30415	4.01038
	Slope	1.66264	0.12092
P-PPIXMnCl (15mg)	Intercept	19.37563	1.39837
	Slope	1.33284	0.04216

Table (C)

Fig. 12. (A) The apparent kinetic curves of reaction (2) and (3) at 10 °C; (B) The apparent kinetic curves of reaction (2) and (3) at 37.5 °C; (C) The apparent kinetic curves of reaction (3) at different amount of catalyst P-PPIXMnCl at 10 °C.

Table 2

The apparent kinetic models of three reactions.

Catalyst	Reaction	Temperature (°C)	Kinetic Equation	$\frac{d(Fe^{3+})}{dt}=k[Fe^{2+}]^m[H_2O_2]^n$ Apparent Rate Constant k	m, n	Reaction Order
Free catalyst	$Fe^{2+}\xrightarrow{H_2O_2}Fe^{3+}$ (1)	10	$\frac{1}{[H_2O_2]_0-[Fe^{2+}]_0}\ln\frac{[Fe^{2+}]_0([H_2O_2]_0-x)}{[H_2O_2]_0([Fe^{2+}]_0-x)}=0.281t+4.99$	0.28	m=1 n=1	Second Order Reaction
		37.5	$\frac{1}{[H_2O_2]_0-[Fe^{2+}]_0}\ln\frac{[Fe^{2+}]_0([H_2O_2]_0-x)}{[H_2O_2]_0([Fe^{2+}]_0-x)}=1.38t+21.4$	1.38		
10 mg manganese porphrins (n(Mn^{3+}): 15.38 μmol)	$Fe^{2+}\xrightarrow[\text{Manganese porphyrin}]{H_2O_2}Fe^{3+}$ (2)	10	$\frac{1}{[H_2O_2]_0-[Fe^{2+}]_0}\ln\frac{[Fe^{2+}]_0([H_2O_2]_0-x)}{[H_2O_2]_0([Fe^{2+}]_0-x)}=1.14t+\text{[illegible]}.52$	1.14	m=1 n=1	Second Order Reaction
		37.5	$\frac{1}{[H_2O_2]_0-[Fe^{2+}]_0}\ln\frac{[Fe^{2+}]_0([H_2O_2]_0-x)}{[H_2O_2]_0([Fe^{2+}]_0-x)}=2.40t+23.8$	2.40		
10 mg P-PPIXMnCl (n(Mn^{3+}): 10.98 μmol)	$Fe^{2+}\xrightarrow[\text{P-PPIXMnCl}]{H_2O_2}Fe^{3+}$(3)	10	$\frac{1}{([Fe^{2+}]_0-[H_2O_2]_0)^2}\left(\ln\frac{[Fe^{2+}]_0-x}{[H_2O_2]_0-x}+\frac{[H_2O_2]_0-[Fe^{2+}]_0}{[Fe^{2+}]_0-x}+\ln\frac{[H_2O_2]_0}{[Fe^{2+}]_0}-\frac{[H_2O_2]_0}{[Fe^{2+}]_0}+1\right)=1.66t+11.3$	1.66	m=2 n=1	Third Order Reaction
		37.5	$\frac{1}{([Fe^{2+}]_0-[H_2O_2]_0)^2}\left(\ln\frac{[Fe^{2+}]_0-x}{[H_2O_2]_0-x}+\frac{[H_2O_2]_0-[Fe^{2+}]_0}{[Fe^{2+}]_0-x}+\ln\frac{[H_2O_2]_0}{[Fe^{2+}]_0}-\frac{[H_2O_2]_0}{[Fe^{2+}]_0}+1\right)=7.29t+25.8$	7.29		
5 mg P-PPIXMnCl (n(Mn^{3+}): 5.49 μmol)	$Fe^{2+}\xrightarrow[\text{P-PPIXMnCl}]{H_2O_2}Fe^{3+}$(3)	10	$\frac{1}{([Fe^{2+}]_0-[H_2O_2]_0)^2}\left(\ln\frac{[Fe^{2+}]_0-x}{[H_2O_2]_0-x}+\frac{[H_2O_2]_0-[Fe^{2+}]_0}{[Fe^{2+}]_0-x}+\ln\frac{[H_2O_2]_0}{[Fe^{2+}]_0}-\frac{[H_2O_2]_0}{[Fe^{2+}]_0}+1\right)=0.363t+0.425$	0.36	m=2 n=1	Third Order Reaction
15 mg P-PPIXMnCl (n(Mn^{3+}): 16.47 μmol)		10	$\frac{1}{([Fe^{2+}]_0-[H_2O_2]_0)^2}\left(\ln\frac{[Fe^{2+}]_0-x}{[H_2O_2]_0-x}+\frac{[H_2O_2]_0-[Fe^{2+}]_0}{[Fe^{2+}]_0-x}+\ln\frac{[H_2O_2]_0}{[Fe^{2+}]_0}-\frac{[H_2O_2]_0}{[Fe^{2+}]_0}+1\right)=1.33t+19.4$	1.33		

Table 3

The E_a (apparent activation energy) and A (diffusion factor) values of the three reactions.

	$Fe^{2+}\xrightarrow{H_2O_2}Fe^{3+}$ (1)	$Fe^{2+}\xrightarrow[\text{Manganese porphyrin}]{H_2O_2}Fe^{3+}$ (2)	$Fe^{2+}\xrightarrow[\text{P-PPIXMnCl}]{H_2O_2}Fe^{3+}$ (3)

		(n (Mn^{3+}): 15.38 μmol)	(n (Mn^{3+}): 10.98 μmol)
E_a	4.43×10^4	2.59×10^4	4.10×10^4
A	3.51×10^7	6.57×10^4	2.37×10^7

To study the possible effect of double bonds on Fe^{2+}, the polymer was added to the Fe^{2+} solution and stirred for 0.5 h in the atmosphere of N_2, the concentration of Fe^{2+} was measured before and after stirring. It was found that the concentration of Fe^{2+} decreased from 0.198 mg/L to 0.189 mg/L after stirring. The result shows that the C=C bonds of polymer chains have the enrichment effect on Fe^{2+} and as a result the local concentration of Fe^{2+} around the catalytic active sites is relatively higher than that in the bulk. Therefore, the oxidation of Fe^{2+} catalyzed by P-PPIXMnCl is a diffusion control process and the increase of reaction order may be ascribed to the coordination effect of C=C bonds in ROMP polymer.

In order to explore the influence of C=C on the oxidation of Fe^{2+} in the reaction, we hydrogenated the carrier PolyNDT, and then loaded manganese porphyrins to get HP-PPIXMnCl to catalyze oxidation of low concentration Fe^{2+}. Fig. 13 shows the apparent kinetic curve of catalytic oxidation of Fe^{2+} by the HP-PPIXMnCl. The catalytic oxidation of Fe^{2+} by HP-PPIXMnCl conforms to the second-order kinetic, which is consistent with the reaction order of manganese porphyrins as catalyst and without catalyst. The result well verifies our conjecture and proves that the apparent reaction kinetic in the reaction process for catalytic oxidation of low concentration Fe^{2+} is influenced by C=C in P-PPIXMnCl. Table (D) in Fig. 15 shows the parameters of the kinetic curve.

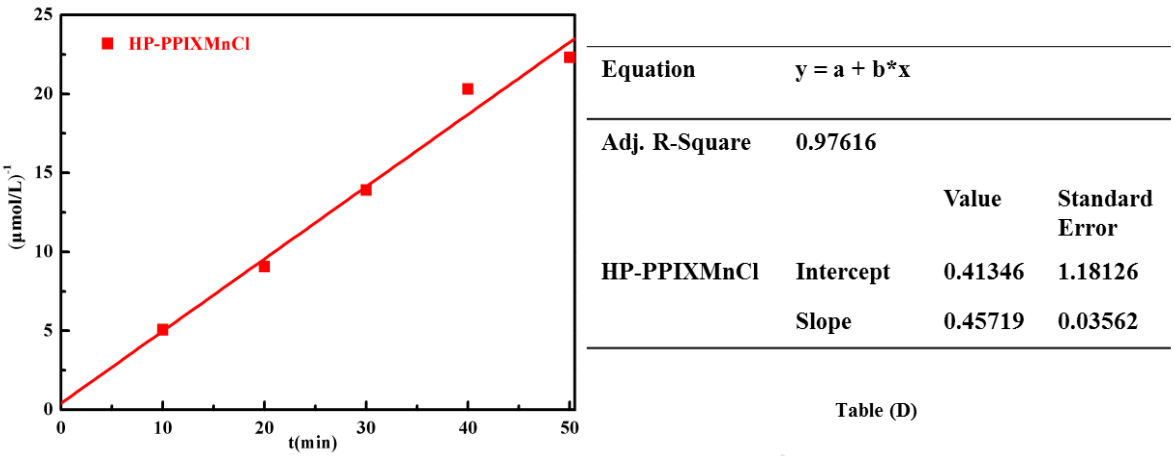

Equation	y = a + b*x		
Adj. R-Square	0.97616		
		Value	Standard Error
HP-PPIXMnCl	Intercept	0.41346	1.18126
	Slope	0.45719	0.03562

Table (D)

Fig. 13. Apparent kinetic curve of reaction catalyzed by HP-PPIXMnCl at 10 °C.

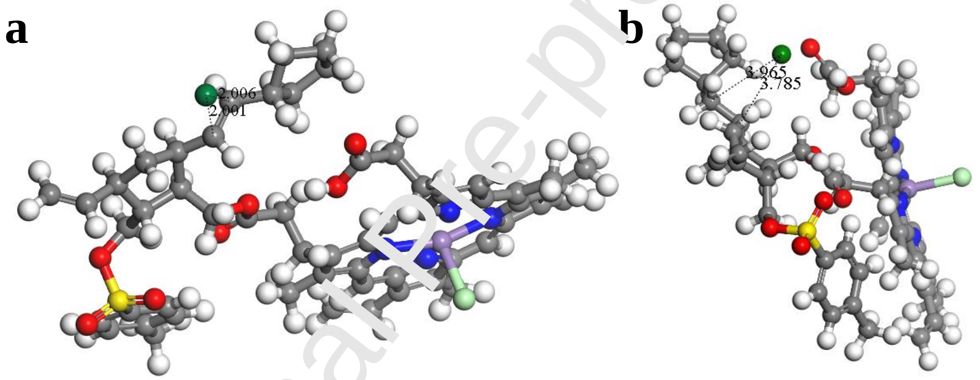

Fig. 14. Optimized structures of Fe^{2+} with C=C of P-PPIXMnCl (a) and with C-C of HP-PPIXMnCl (b).

Table 4

The calculated interaction energy E_{inter} of Fe^{2+} and ploymers.

Ploymers	E_{inter} (kJ·mol^{-1})
P-PPIXMnCl	-840.4
HP-PPIXMnCl	-302.8

The Optimized structures of Fe^{2+} with C=C of P-PPIXMnCl (a) and with C-C of HP-PPIXMnCl (b) are shown in Fig. 14. And the corresponding energies are listed in Table 4. The absolute value of interaction energy between Fe^{2+} and C=C of P-PPIXMnCl (a) (840.4 kJ·mol^{-1}) is larger than that of Fe^{2+} and

C-C of HP-PPIXMnCl (b) (302.8 kJ·mol^{-1}). What's more, the distance between Fe^{2+} and C-C is larger than that of Fe^{2+} and C=C. In summary, larger absolute value of interaction energy as well as shorter interatomic distance means the stronger interaction. These outcomes indicate that C=C has a stronger interaction with Fe^{2+} so that the substrate Fe^{2+} gathers near the carrier and influences the reaction process of catalytic oxidation of the substrate. This phenomenon is consistent with the kinetic experiment results.

3.3. Catalyst recycling

The recyclability of P-PPIXMnCl was examined using the oxidation of Fe^{2+}. The particles were separated at the end of the reaction by centrifugation, washed and reused six times. Fig. 15 shows that the P-PPIXMnCl is effective on the first three consecutive runs, the conversion rates are all above 90%. By the sixth cycle, conversion rate of Fe^{2+} was 88.29%. They showed outstanding reusability without significant catalytic activity losses, and the slightly reduced conversion rate (α (%)) of Fe^{2+} is attributed to the very slow decomposition of the catalytic system in the oxidizer. The filtrate was also examined by UV-Vis spectrophotometer for the presence of the manganese porphyrins after each recycling experiment (Fig. S10). No detectable trace of manganese porphyrins is detected in the range 300-800 nm (compare with line c in Fig. S9), and that confirms the absence of the manganese porphyrins in the filtrate. The results have strongly explained that it is induced by the better stabilization of the manganese porphyrins after immobilizing. In general, the control experiments indicate that the observed catalytic results are obtained from the heterogeneous catalysts. Moreover, there is no active component leaching in the catalytic process. These data are consistent with the results of catalyst activity in cyclic experiments.

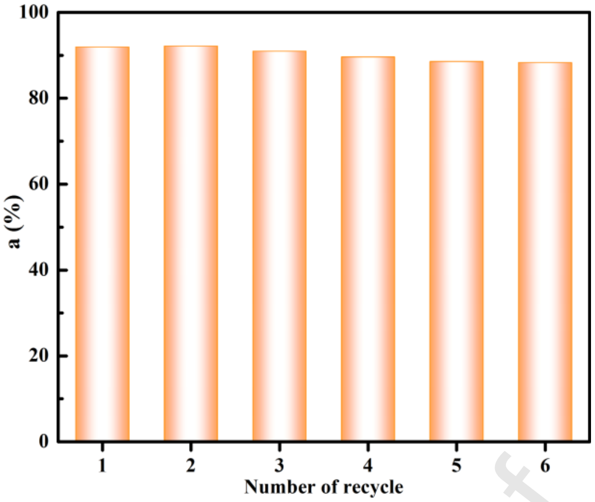

Fig. 15. Catalytic activity of the recovered catalyst. Recycling reaction conditions: P-PPIXMnCl 10 mg, Fe^{2+} solution (3.53 μmol/L), H_2O_2 (32.65 mmol/L) at 10 °C for 50 min.

4. Conclusions

ROMP of norbornene-2,3-dip-toluene sulfonate is initiated by the Grubbs 2nd catalyst and manganese porphyrins are successfully immobilized onto ROMP unsaturated polymer. The supported catalyst (P-PPIXMnCl) can effectively catalyze oxidation of low concentration Fe^{2+} at low temperature. Because polymer support overcomes agglomeration of manganese porphyrins, the diffusion resistance is in the same order of magnitude with homogeneous reaction. In the presence of P-PPIXMnCl, the oxidation reaction changes from second-order to third-order due to coordination effect of C=C bonds along polymer chains. Upon hydrogenation of ROMP polymer, the oxidation reaction still conforms to the second-order kinetic. And the interaction force between Fe^{2+} and C=C of P-PPIXMnCl is larger than that between Fe^{2+} and C-C of HP-PPIXMnCl according to DFT calculation. Therefore, the C=C bonds along polymer chains play an important role through the coordination with Fe^{2+} in the catalytic microenvironment. Morever, The ture morphology of P-PPIXMnCl and HP-PPIXMnCl in aqueous environment characterized by Cryo-TEM indicate that hydrogenation can shrink the morphology of polymer-water skeleton. It is well explained that the C=C bonds along polymer chains provides a flexible microenvironment for the active center of the catalyst so as to give full play to the catalytic performance of the catalyst. The catalyst P-PPIXMnCl in the aqueous solution could be recycled to oxidize Fe^{2+}, and conversion rate of Fe^{2+} reduced slightly after six recycles, from 91.92% to 88.29%. From the studies of UV-Vis spectra, we speculate that this is induced by the better stabilization of the manganese porphyrins after immobilizing. Therefore, P-PPIXMnCl is one potential candidate of Cp to maintain the iron homeostasis of the body.

Data availability

The raw/processed data required to reproduce these findings cannot be shared at this time as the data also forms part of an ongoing study.

Declaration of Competing Interest

The authors declare no competing financial interest.

Author information

Corresponding Author

*E-mail: zhangyanwu@zzu.edu.cn

ORCID

Yanwu Zhang: 0000-0002-5441-9961

Acknowledgments

We gratefully acknowledge the financial support from the National Natural Science Foundation of China (21574119). We thank the Supercomputing Center in Zhengzhou University (Zhengzhou, China).

References

[1] J. R. L. Smith, Y. Iamamoto, F. S. Vinhado, Oxidation of alkanes by iodosylbenzene (PhIO) catalysed by supported Mn (III) porphyrins: Activity and mechanism, J. Mol. Catal. A-Chem. 252 (2006) 23-30.

[2] J. Połtowicz, K. Pamin, E. Tabor, J. Haber, A. Adamski, Z. Sojka, Metallosalen complexes immobilized in zeolite NaX as catalysts of aerobic oxidation of cyclooctane, Appl. Catal. A-Gen. 299 (2006) 235-242.

[3] S. L. Rebelo, A. R. Gonçalves, M. M. Pereira, M. M. Simões, M. G. P. Neves, J. A. Cavaleiro, Epoxidation reactions with hydrogen peroxide activated by a novel heterogeneous metalloporphyrin catalyst, J. Mol. Catal. A-Chem. 256 (2006) 321-323.

[4] C. P. Du, Z. K. Li, X. M. Wen, J. Wu, X. Q. Yu, M. Yang, R. G. Xie, Highly diastereoselective epoxidation of cholest-5-ene derivatives catalyzed by polymer-supported manganese (III) porphyrins, J. Mol. Catal. A-Chem. 216 (2004) 7-12.

[5] X. T. Zhou, Q. H. Tang, H. B. Ji, Remarkable enhancement of aerobic epoxidation reactivity for olefins catalyzed by μ-oxo-bisiron (III) porphyrins under ambient conditions, Tetrahedron Lett. 50 (2009) 6601-6605.

[6] C. Crestini, R. Saladino, P. Tagliatesta, T. Boschi, Biomimetic degradation of lignin and lignin model compounds by synthetic anionic and cationic water soluble manganese and iron porphyrins, Bioorg. Med. Chem. 7 (1999) 1897-1905.

[7] H. Kolarova, J. Macecek, P. Nevrelova, M. Huf, M. Tomecka, R. Bajgar, M. strnad, Photodynamic therapy with zinc-tetra (p-sulfophenyl) porphyrin bound to cyclodextrin induces single strand breaks of cellular DNA in G361 melanoma cells, Toxicol.Vitro. 19 (2005) 971-974.

[8] C. D. Vulpe, Y. M. Kuo, T. L. Murphy, L. Cowley, C. Askwith, N. Libina, G. J. Anderson, Hephaestin, a ceruloplasmin homologue implicated in intestinal iron transport, is defective in the sla mouse, Nature Genet. 21 (1999) 195-199.

[9] S. Cherukuri, R. Potla, J. Sarkar, S. Nurko, Z. L. Harris, P. L. Fox, Unexpected role of ceruloplasmin in intestinal iron absorption, Cell Metab. 2 (2005) 309-319.

[10] G. Musci, M. C. B. di Patti, L. Calabrese, Modulation of the redox state of the copper sites of human ceruloplasmin by chloride, J.Protein Chem. 14 (1995) 611-619.

[11] G. Floris, R. Medda, A. Padiglia, G. Musci, The physiopathological significance of ceruloplasmin: a possible therapeutic approach, Biochem. Pharmacol. 60 (2000) 1735-1741.

[12] V. N. Zaitsev, I. Zaitseva, M. Papiz, P. F. Lindley, An X-ray crystallographic study of the binding sites of the azide inhibitor and organic substrates to ceruloplasmin, a multi-copper oxidase in the plasma, J. Biol. Inorg. Chem. 4 (1999) 579-587.

[13] P. F. Lindley, G. Card, I. Zaitseva, V. Zaitsev, B. Reinhammar, E. Selin-Lindgren, K. Yoshida, An X-ray structural study of human ceruloplasmin in relation to ferroxidase activity, J. Biol. Inorg. Chem. 2 (1997) 454-463.

[14] Z. L. Harris, A. P. Durley, T. K. Man, J. D. Gitlin, Targeted gene disruption reveals an essential role for ceruloplasmin in cellular iron efflux, Proc. Natl. Acad. Sci. 96 (1999) 10812-10817.

[15] G. Yin, Understanding the oxidative relationships of the metal oxo, hydroxo, and hydroperoxide intermediates with manganese (IV) complexes having bridged cyclams: Correlation of the physico-chemical properties with reactivity, Accounts Chem. Res. 46 (2012) 483-492.

[16] J. C. Barona-Castaño, C. C. Carmona-Vargas, T. J. Brocksom, K. T. De Oliveira, Porphyrins as catalysts in scalable organic reactions, Molecules. 21 (2016) 310.

[17] A. B. Sorokin, Phthalocyanine metal complexes in catalysis, Chem. Rev. 113 (2013) 8152-8191.

[18] B. Li, C. Zheng, H. Liu, J. Zhu, H. Zhang, D. Gao, W. Huang, (2016). Large planar π- conjugated porphyrin for interfacial engineering in pin perovskite solar cells, ACS Appl. Mater. Inter. 8 (2016) 27438-27443.

[19] S. Shaik, S. Cohen, Y. Wang, H. Chen, D. Kumar, W. Thiel, P450 enzymes: Their structure, reactivity, and selectivity□ modeled by QM/MM calculations, Chem. Rev. 110 (2009) 949-1017.

[20] S. haik, S. Cohen, Y. Wang, H. Chen, D. Kumar, W. Thiel, P450 enzymes: Their structure, reactivity, and selectivity□ modeled by QM/MM calculations, Chem. Rev. 110 (2009) 949-1017.

[21] M. Espinosa, S. acheco, R. Rodriguez, Synthesis and characterization of NH2-porphyrins covalently immobilized on modified-SBA-15, J. Non-Cryst. Solids. 353 (2007) 2573-2581.

[22] J. Połtowicz, K. Pamin, L. Matachowski, E. M. Serwicka, R. Mokaya, Y. Xia, Z. Olejniczak, Oxidation of cyclooctane over Mn (TMPyP) porphyrin-exchanged Al, Si-mesoporous molecular sieves of MCM-41 and SBA-15 type, Catal. Today. 114 (2006) 287-292.

[23] Q. Zhu, S. Maeno, R. Nishimoto, T. Miyamoto, M. Fukushima, Oxidative degradation of pentabromophenol in the presence of humic substances catalyzed by a SBA-15 supported iron-porphyrin catalyst, J. Mol. Catal. A-Chem. 385 (2014) 31-37.

[24] F. C. Skrobot, I. L. Rosa, A. P. A. Marques, P. R. Martins, J. Rocha, A. A. Valente, Y. Iamamoto, Asymmetric cationic methyl pyridyl and pentafluorophenyl porphyrin encapsulated in zeolites: A cytochrome P-450 model, J. Mol. Catal. A-Chem. 237 (2005) 86-92.

[25] O. J. de Lima, D. P. de Aguirre, D. C. de Oliveira, M. A. da Silva, C. Mello, C. A. Leite, K. J. Ciuffi, Porphyrins entrapped in an alumina matrix, J. Mater. Chem. 11 (2001) 2476-2481.

[26] M. Moghadam, S. Tangestaninejad, V. Mirkhani, I. Mohammadpoor-baltork, N. Sirjanian, S. Parand, Polystyrene-bound Mn (T4PyP): A highly efficient and reusable catalyst for biomimetic oxidative decarboxylation of carboxylic acids with sodium periodate, Bioorg. Med. Chem. 17 (2009) 3394-3398.

[27] E. Brulé, Y. R. de Miguel, K. K. M. Hii, Chemoselective epoxidation of dienes using polymer-supported manganese porphyrin catalysts, Tetrahedron. 60 (2004) 5913-5918.

[28] B. Meunier, Metalloporphyrins as versatile catalysts for oxidation reactions and oxidative DNA cleavage, Chem. Rev. 92 (1992) 1411-1456.

[29] D. Mansuy, A brief history of the contribution of metalloporphyrin models to cytochrome P450 chemistry and oxidation catalysis, C. R. Chim. 10 (2007) 392-413.

[30] S. Nakagaki, G. KB Ferreira, A. L Marcalo, K. J Ciuffi, Metalloporphyrins immobilized on silica and modified silica as catalysts in heterogeneous processes, Curr. Org. Synth. 11 (2014) 67-88.

[31] E. Brulé, Y. R. de Miguel, Supported manganese porphyrin catalysts as P450 enzyme mimics for alkene epoxidation, Tetrahedron Lett. 43 (2002) 8555-8558.

[32] G. Qiu, X. Liu, B. Wang, H. Gu, W. Wang, Ferrocene-containing amphiphilic polynorbornenes as biocompatible drug carriers, Polymer Chem. 10 (2019) 2527-2539.

[33] X. Liu, F. Liu, D. Astruc, W. Lin, H. Gu, Highly-branched amphiphilic organometallic dendronized diblock copolymer: ROMP synthesis, self-assembly and long-term Au and Ag nanoparticle stabilizer for high-efficiency catalysis, Polymer. 173 (2019) 1-10.

[34] G. I. Peterson, K. T. Bang, T. L. Choi, Mechanochemical Degradation of Denpols: Synthesis and Ultrasound-Induced Chain Scission of Polyphenylene-Based Dendronized Polymers, J. Am. Chem. Soc. 140 (2018) 8599-8608.

[35] X. Liu, W. Lin, D. Astruc, H. Gu, Syntheses and applications of dendronized polymers, Prog. Polym. Sci. 96 (2019) 43-105.

[36] M. Yasir, P. Liu, I. K. Tennie, A. F. Kilbinger, Catalytic living ring-opening metathesis polymerization with Grubbs' second-and third-generation catalysts, Nat. Chem. 11 (2019) 488.

[37] X. Liu, F. Liu, Y. Wang, H. Gu, Ferrocene-containing amphiphilic dendronized random copolymer as efficient stabilizer for reusable gold nanoparticles in catalysis, React. Funct. Polym. 143 (2019) 104325.

[38] Y. Sha, M. A. Rahman, T. Zhu, Y. Cha, C. W. McAlister, C. Tang, ROMPI-CDSA: ring-opening metathesis polymerization-induced crystallization-driven self-assembly of metallo-block copolymers, Chem. Sci. 10 (2019) 9782-9787.

[39] S. Dhawan, M. B. Bijesh, V. Haridas, Polymersomes from hybrid peptide-based bottlebrush homopolymers, Polymer. 138 (2018) 218-228.

[40] B. J. Wilson, J. N. Brantley, Synthesis and Reactivity of Metallocarbene-Containing Polymers, J. AM. Chem. Soc. 141 (2019) 12453-12457.

[41] P. Bertrand, C. Blanquart, V. Héroguez, The ROMP: A Powerful Approach to Synthesize Novel pH-Sensitive Nanoparticles for Tumor Therapy, Biomolecules. 9 (2019) 60.

[42] I. Choinopoulos, Grubbs' and Schrock's Catalysts, Ring Opening Metathesis Polymerization and Molecular Brushes-Synthesis, Characterization, Properties and Applications, Polymers. 11 (2019) 298.

[43] E. Rose, B. Andrioletti, S. Zrig, M. Quelquejeu-Ethève, Enantioselective epoxidation of olefins with chiral metalloporphyrin catalysts, Chem. Soc. Rev. 34 (2005) 573-583.

[44] F. Xu, J. Jing, X. Zhou, Y. Zhang, Bifunctional Chelating Supramolecular Polymer and Its Application in Downregulation of Cellular Iron Uptake, Biomacromolecules. 18 (2017) 2830-2838.

[45] B. Engın, M. Guru, A. Alıcılar, Removal of Ferrous Ion in Synthetic Waters by Catalytic Air Oxidation, Asian J. Chem. 21 (2009) 2067-2072.

[46] R. P. Azar, C. Falamaki, Removal of Aqueous Fe^{2+} Using MnO$_2$-Clinoptilolite in a Batch Slurry Reactor: Catalyst Synthesis, Characterization and Modeling of Catalytic Behavior, J. Ind. Eng. Chem. 18 (2012) 737-743.

[47] W. Stumm, G. F. Lee, Oxygenation of Ferrous Iron, Ind. Eng. Chem. 53 (1961) 143-146.

[48] N. Pal, N. Kumar, A. Mandal, Stabilization of Dispersed Oil Droplets in Nanoemulsions by Synergistic Effects of the Gemini Surfactant, PHPA Polymer, and Silica Nanoparticle, Langmuir. 35 (2019) 2655-2667.

[49] K. V. Bukhryakov, V. G. Desyatkin, J. P. O'Shea, S. R. Almahdali, V. Solovyeva, V. O. Rodionov, Cooperative catalysis with block copolymer micelles: A combinatorial approach, ACS Comb. Sci. 17 (2015) 76-80.

[50] T. M. Eggenhuisen, H. Friedrich, F. Nudelman, J. Zečević, N. A. Sommerdijk, P. E. de Jongh, K. P. de Jong, Controlling the distribution of supported nanoparticles by aqueous synthesis, Chem. Mat. 25 (2013) 890-896.

[51] W. Liu, J. T. Groves, Manganese porphyrins catalyze selective C-H bond halogenations, J. Am. Chem. Soc. 132 (2010) 12847-12849.

[52] A. Bergner, M. Dolg, W. Küchle, H. Stoll, H. Preuß, Ab initio energy-adjusted pseudopotentials for elements of groups 13-17, Mol. Phys. 80 (1993) 1431-1441.

[53] C. K. Chu, T. P. Lin, H. Shao, A. L. Liberman-Martin, P. Liu, R. H. Grubbs, Disentangling Ligand Effects on Metathesis Catalyst Activity: Experimental and Computational Studies of Ruthenium-Aminophosphine Complexes, J. Am. Chem. Soc. 140 (2018) 5634-5643.

[54] A. M. D. A. R. Gonsalves, A. C. Serra, On the Mechanism of Carboxylic acid Co-catalyst assisted Metalloporphyrin Oxidations, J Mol Catal A-Chem.168 (2001) 25-32.

[55] A. C. Serra, E. C. Marçalo, A. D. A. R. Gonsalves, A view on the mechanism of metalloporphyrin degradation in hydrogen peroxide epoxidation reactions, J Mol Catal A-Chem. 215 (2004) 17-21.

[56] C. Crestini, R. aladino, P. Tagliatesta, T. Boschi, Biomimetic degradation of lignin and lignin model compounds by synthetic anionic and cationic water soluble manganese and iron porphyrins, Bioorgan. Med. Chem. 7 (1999) 1897-1905.

[57] T. C. Bruice, Reactions of hydroperoxides with metallotetraphenylporphyrins in aqueous solutions, Accounts Chem. Res. 24 (1991) 243-249.

[58] P. N. Balasubramanian, E. S. Schmidt, T. C. Bruice, Catalase modeling. 2. Dynamics of Reaction of a Water-Soluble and Non μ-Oxo Dimer Forming Manganese (III) Porphyrin with Hydrogen Peroxide, J. Am. Chem. Soc. 109 (1987) 7865-7873.

Author Statement

All authors have seen and approved the final version of the manuscript being submitted. All the authors warrant that the work is the authors' original work, hasn't received prior publication and isn't under consideration for publication elsewhere.

Conflict of Interest

All the other authors listed have approved the manuscript that is enclosed and declare no conflict of interest.

Graphical Abstract

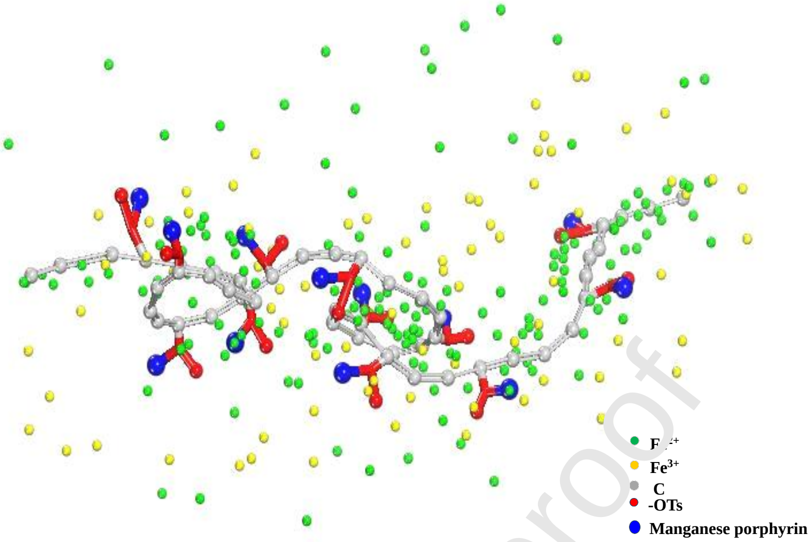

Highlights

- Manganese porphyrins were supported on ROMP polymer to mimic ceruloplasmin.
- The oxidation behavior of low concentration Fe^{2+} catalyzed by supported manganese porphyrins is studied at low temperature.
- The catalytic activity of manganese porphyrins are enhanced by the flexible microenvironment of the polymer chain.
- The catalytic kinetic of reaction catalyzed by supported manganese porphyrins changes from second-order to third-order.
- The apparent reaction kinetic of the reaction is influenced by C=C of polymer carrier.